Journal of Molecular Structure xxx (xxxx) xxx

Contents lists available at ScienceDirect

Journal of Molecular Structure

journal homepage: www.elsevier.com/locate/molstr

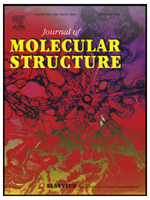

Synthesis and physicochemical characterization of Schiff bases used as optical sensor for metals detection in water

Cesar Garcias-Morales[a,*], Josué Espinosa Maldonado[a], Armando Ariza Castolo[b], Catalina M. Perez Berumen[a], Marco Antonio Lobato[a], Mario Alejandro Rodriguez[c], Arian Espinoza Roa[d]

[a] Departamento de Química Orgánica, Facultad de Ciencias Químicas, Universidad Autónoma de Coahuila, 25280 Saltillo, Coahuila, Mexico
[b] Departamento de Química, Centro de Investigación y de Estudios Avanzados del Instituto Politécnico Nacional, Avenida Instituto Politécnico Nacional 2508 Colonia San Pedro Zacatenco, 07360 Mexico, D.F., Mexico
[c] Research Group of Optical Properties of Materials (GPOM), Centro de Investigaciones en Óptica, A.P. 1-948, 37000 León, Guanajuato, México
[d] CONACYT-Centro de Investigación en Química Aplicada Unidad Monterrey Apodaca México

ARTICLE INFO

Article history:
Received 16 July 2020
Revised 9 October 2020
Accepted 11 October 2020
Available online xxx

Keywords:
Imines
Optical sensors
Metal ions
Aqueous medium
DFT calculations
Smart design

ABSTRACT

In this work, chemical mechanic synthesis of six imines is reported, chemical structure and optical characterization is described. The imines **3a-3f** were evaluated as colorimetric chemical sensors of metals: Ba^{2+}, Co^{2+}, Fe^{2+}, Mg^{2+}, Ni^{2+}, Pb^{2+}, Zn^{2+}, Cd^{2+}, Hg^{2+}, Cu^{2+}, Sn^{2+} and Cs^{+} where **3e** being a highly selective colorimetric chemical sensor for Cu^{2+}. The limit detection of the sensor was determined through the titration, which turned out to be 4.9×10^{-6} M with a Ka of 8.264×10^{3} M^{-1}. Also, the interference of detection in a mixture of metals was studied. Finally, by the use of IR, NMR, and DFT calculations, the structure of the **3e + M** complex formed, and the phenomenon responsible for the color change was determined. Finally, a possible relationship between the selectivity to metal ions and the HOMO energy levels of the molecules is proposed, being a basis for the design of smart organic sensors

© 2020 Elsevier B.V. All rights reserved.

1. Introduction

In the last two decades, organic chemical sensors development has attracted attention because they are cheap and easy to synthesize. Some chemical sensors are based on optical detection either by colorimetric or fluorescence [1,2]. Many optical chemical sensors have been synthesized whose design depends on the substance to be detected. Within the organic chemical sensors that have been developed are found; gas sensors [3], explosive chemical sensors [4–6], metabolite and peptide sensors [7,8], carbohydrate sensors [9,10], ion sensors [11–13], among others [14].

Organic chemical sensors for metal ions detection as; Hg^{2+}, Cu^{2+}, Zn^{2+}, Fe^{2+}, Mn^{2+}, Co^{2+}, Pb^{2+}, and Cd^{2+}, have been studied extensively since at low exposure levels, they cause neurological, reproductive, and cardiovascular problems [15,16]. A developmental disorder that mainly affects children induces a low motor response, decreased IQ, and hypertension; several of these metals are also carcinogenic substances [17,18].

Chemical sensors use the molecular recognition to coordinate the metals, the interaction between the chemical sensor and metal; can be through coordination or electrostatic interactions. One advantage of organic optical sensors is their sensitivity since they can detect samples even in concentrations of 1×10^{-7} M. The coordination between the organic molecule and the metal ion causes an electronic density rearrangement through internal charge formation transfer complexes (ICT). This ICT causes changes in the energy band-gap of molecules, changing the UV-Vis absorption and, therefore, in molecule color [19].

The main advantage of chemical sensors over other metals detection methods is the simplicity of the synthesis, the high sensitivity and selectivity that can be achieved, and their low cost. Fluorescent chemo-sensors have been reported using pyrenes derivatives [20], calixarenes [21], benzimidazole [22], and rhodamine [23–25]. Czarnik et al. reported molecules derived from anthracene used as fluorescent chemo-sensors in the Pb^{2+} detection [26]. Metal ion detection for this method is easy to interpret. In solution, the molecules described are not fluorescent; however, when

---

[*] Corresponding author.
E-mail address: cgarcias@uadec.edu.mx (C. Garcias-Morales).

https://doi.org/10.1016/j.molstruc.2020.129444
0022-2860/© 2020 Elsevier B.V. All rights reserved.

coordinated with Pb^{2+}, they are highly fluorescent due to a photo-induced electronic transfer, which indicates the Pb^{2+} presence.

Some compounds derived from rhodamine B [27], have been used as colorimetric and fluorescent chemo-sensors for Pb^{2+} detection; these compounds showed high selectivity and detection at low concentrations (1 mM) using perchlorate salts of Ag^+, Ca^{2+}, Cd^{2+}, Co^{2+}, Cs^+, Cu^{2+}, Hg^{2+}, K^+, Li^+, Mg^{2+}, Mn^{2+}, Na^+, Ni^{2+}, Pb^{2+}, Rb^+ and Zn^{2+} in acetonitrile [28]. Chalcones have also been reported as selective colorimetric chemo-sensors for Cu^{2+}, Ni^{2+}, and Cd^{2+} in a mixture of CH_3CN/H_2O (95/5, v/v) [29]. The structure of the L+M coordination complex in these compounds was studied by IR and NMR spectroscopy. It was determined that metal coordination with the molecule is through the lone pair electrons of nitrogen (nN) and oxygen (nO).

The Schiff bases have attracted attention due to its easy preparation and purification, considering its since its synthesis is inherent to the 12 principles of green chemistry [30]. Have a high atomic economy since the reaction proceeds only with water as a byproduct; its structures are easily adjustable and efficiently degraded after use; therefore, they are promising molecules as chemical sensors [31–34]. Rodriguez et al. reported π-conjugated imines derived from N,N'-dimethyl cinnamaldehyde. These molecules are colorimetric sensors of Cu^{2+} and Ni^{2+}, with detection limits of 0.125 μM [35,36].

The Cu^{2+} detection in water for human consumption is essential because a high concentration of this metal is related to Alzheimer's and Parkinson's disease [37,38] (since copper regularly coordinates proteins by changing its folding and aggregation properties). Consequently, developing a highly selective chemo-sensor to this metal is of great importance, enabling easy detection in real-time.

In this work, the synthesis of six Schiff bases derivatives (**3a-3f**), which functions as a colorimetric chemical-sensor for metal detections, is described. The chemical-sensors **3e** can detect Cu^{2+} at concentrations of 4.9×10^{-6} M, in aqueous solution. The addition of the aqueous metal ion (**M**) to the sensor 3e (L) solution in CH_3CN causes an optical change since the initially colorless solution changes to yellow when forming the **L+M** complex. UV-Visanalysis showed the formation of two absorption bands at 406 and 420 nm, both attributed to the ICT of the **L+M** complex. The relationship between the structure, the HOMO-LUMO energy levels, and the selectivity to metal ions was also studied.

2. Experimental section

All reagents and chemicals were used without further purification unless stated otherwise. The salts used to prepare the solutions were: $Zn(ClO_4)_2·6H_2O$, $Ni(ClO_4)_2·6H_2O$, $CoCl_2·6H_2O$, $Mg(ClO_4)_2$, $Pb(ClO_4)_2·3H_2O$, $FeCl_2·4H_2O$, $Cu(ClO_4)_2·6H_2O$, $Ba(ClO_4)_2$, $Cd(ClO_4)_2$, and $Hg(ClO_4)_2$. The salts of metals, organic solvents, 2-hydroxymethyl aniline, 2-formyl pyrrole, 2-thiophenecarboxaldehyde, salicylaldehyde, 2,6-diaminopyridine, 3,5-diamino-1,2,4-triazole, 4-nitroaniline, 2,4-dimethoxyaniline, were purchased from Aldrich.

The infrared spectra were obtained using a Perkin-Elmer 16F PC FT-IR spectrometer, using the ATR technique in a range of 4000-500 cm^{-1}. Nuclear magnetic resonance spectra of ^1H and ^{13}C were obtained in a Jeol/ECA at 500 MHz for ^1H and 125 MHz for ^{13}C. The chemical shift is expressed in ppm using $Si(CH_3)_4$ as internal reference ($\delta = 0$ ppm) and $CDCl_3$ as a solvent. The high-resolution MS spectra were obtained by direct insertion in an Agilent G1969 LC/MSD-TOF. The UV-Vis absorption spectra were obtained in a Jenway model 7315 spectrophotometer, using a 1cm cell and a stock solution of 10 μM in acetonitrile analytical grade. Simultaneously, the salts were prepared in a concentration of 10 μM, using distilled and deionized water.

2.1. Synthesis

2.1.1. General procedure

The corresponding amine was placed in a porcelain mortar, and the aldehyde was subsequently added. The reaction was ground for 30 min at room temperature. The reaction was monitored by thin-layer chromatography and was terminated when no change in products and reagents was observed. In all cases, a paste was obtained. After the reaction, ethyl acetate was added. The mixture was cooled to 3°C to purify by recrystallization. The solid was recovered by filtration and dried at room temperature using a stream of nitrogen.

2.1.2. 2-(((2,4-dimethoxyphenyl)imino)methyl)phenol (3a)

In a porcelain mortar 0.30 g (2.0 mmol) of 2,4-dimethoxyaniline and 0.24g (2 mmol) of salicylaldehyde were placed, and then the general procedure was followed. A brown viscous liquid was obtained; yield: 88%, IR (ATR, cm^{-1}): 3371 (OH), 1640 (C=N), 1455 (C=C). ^1H NMR ($CDCl_3$, 500 MHz, δ): 8.7 (s, 1H, H9), 7.3 (m, 2H, H12 and H14), 7.2 (d, 1H, H6), 7.0 (d, 1H, H15), 6.9 (t, 1H, H13), 6.5 (m, 2H, H5 and H3), 3.9 (s, 3H, H8), 3.8 (s, 3H, H7). ^{13}C NMR ($CDCl_3$, 125 MHz, δ): 161.4 (C11), 159.9 (C4), 159.5 (C=N), 154.3 (C2), 132.4 (C13), 131.6 (C15), 130.1 (C10), 119.7 (C6), 119.7 (C1), 118.6 (C4), 117.2 (C12), 99.4 (C3), 55.8 (C7), 55.5 (C8). $[M+H]^+$ $C_{15}H_{15}NO_3$ calculated: 258.112469, [M+H]+ $C_{15}H_{15}NO_3$ found: 258.1127467.

2.1.3. 2-(((4-nitrophenyl)imino)methyl)phenol (3b)

In a porcelain mortar 0.276 g (2.0 mmol) of 4-nitroaniline and 0.24g (2 mmol) of salicylaldehyde were placed, and then the general procedure was followed. An orange solid was obtained; yield: 86%, mp: 121.7 °C, IR (ATR, cm^{-1}): 3479 (N-H), 3356 (OH), 1655 (C=N), 1588 (N-H), 1480 (C=C). ^1H NMR (500 MHz, DMSO-d_6) δ 12.33 (s, 1H, O-H), 8.97 (s, 1H, H7), 8.32 – 8.24 (m, 2H, H3, H5), 7.72 (dd, J = 8.1, 1.7 Hz, 1H, H13), 7.62 – 7.53 (m, 2H, H6 and H2), 7.46 (td, J = 7.7, 1.8 Hz, 1H, H11), 7.00 (m, 2H, H10 and H12). ^{13}C NMR (125 MHz, DMSO-d_6) δ 166.05 (C=N), 160.75 (C9), 154.97 (C1), 145.86 (C4), 134.79 (C11), 132.95 (C13), 125.49 (C2 and C6), 122.90 (C3 and C5), 119.91 (C10), 119.81 (C8), 117.23 (C12). $[M+H]^+$ $C_{13}H_{10}N_2O_3$ calculated: 242.06914, $[M+H]^+$ $C_{13}H_{10}N_2O_3$ found: 242.06916.

2.1.4. ((1H-1,2,4-triazole-3,5-diyl)bis(azanylylidene))bis(methanylylidene))diphenol (3c)

In a porcelain mortar 0.30 g (3.0 mmol) of 3,5-diamino-1,2,4-triazole and 0.74 g (6 mmol) of salicylaldehyde were placed, and then the general procedure was followed. A yellow powder was obtained; yield: 76%; mp: 227 °C, IR (ATR, cm^{-1}): 3389 (N-H) 3200 (O-H), 2298 (C-H), 1570 (N-H), 1471 (C=C). ^1H NMR (500 MHz, DMSO-d_6) δ 12.78 (s, 1H, NH), 12.14 (s, 2H, OH), 9.13 (s, 2H, H2), 7.67 – 7.62 (m, 2H, H8), 7.44 – 7.33 (m, 2H, H6), 6.92 (m, 4H, H7 and H5). ^{13}C NMR (126 MHz, DMSO-d_6) δ 163.71 (C=N), 160.77 (C4), 157.28 (C1), 134.04 (C8), 133.03 (C6), 119.88 (C3), 119.64 (C7), 117.15 (C5). $[M+H]^+$ $C_{16}H_{13}N_5O_2$ calculated: 307.10692, $[M+H]^+$ $C_{16}H_{13}N_3O_2$ found: 282.279689 (loss of N_2).

2.1.5. 2,2′-((1E,1′E)-(pyridine-2,6-diylbis(azanylylidene))bis(methanylylidene))diphenol (3d)

In a porcelain mortar 0.30 g (2.7 mmol) of 2,6-Diaminopyridine and 0.64 g (5.4 mmol) of salicylaldehyde were placed, and then the general procedure was followed. An orange powder was obtained, yield: 85%; mp: 167 °C, IR (ATR, cm^{-1}): ^1H NMR (500 MHz, $CDCl_3$) δ 13.42 (s, OH), 9.47 (s, 2H, H7), 7.82 (t, J = 7.7 Hz, 1H, H10), 7.58 – 7.51 (m, 2H, H6), 7.45 – 7.36 (m, 2H, H4), 7.27 – 7.19

(m, 2H, H9), 7.04 (dd, J = 8.3, 1.0 Hz, 2H, H3), 6.97 (m, 2H, H5). ^{13}C NMR (126 MHz, $CDCl_3$) δ 165.17 (C=N), 162.08 (C2), 156.89 (C8), 140.77 (C10), 134.21 (C6), 133.68 (C4), 119.39 (C5), 119.30 (C3), 119.02 (C1), 117.48 (C9). $M+H]^+$ $C_{19}H_{15}N_3O_2$ calculated: 318.11978, $[M+H]^+$ $C_{19}H_{15}N_3O_2$ found: 318.11996.

2.1.6. 2-(((1H-pyrrol-2-yl)methylene)amino)phenyl)methanol (3e)

In a porcelain mortar 0.30 g (2.4 mmol) of 2- (hydroxymethyl) aniline and 0.22 g (2.4 mmol) of 2-formylpyrrole were placed, and then the general procedure was followed. A gray powder was obtained;yield: 93%; mp: 72 °C; IR (ATR, cm^{-1}): 3402 (N-H), 3366 (OH), 1619 (C=N), 1575 (N-H), 1447 (C=C), 1413 (C-N), 1028 (C-O). ^{1}H NMR ($CDCl_3$, 500 MHz, δ): 11.01 (s, OH), 8.2 (s, 1H, H8), 7.3 (m, 2H, H3 and H5), 7.2 (t, 1H, H4), 7.1 (d, 1H, H6), 6.9 (d, 1H, H12), 6.7 (dd, 1H, H10), 6.3 (dd, 1H, H11), 4.8 (s, 2H, H7); ^{13}C NMR (CDCl, 125 MHz, δ): 149.7 (C2), 149.6 (C8), 134.4 (C1), 130.4 (C9), 128.8 (C6), 128.3 (C5), 125.7 (C4), 124.4 (C12), 118.1 (10), 117.8 (C3), 110.6 (C11), 63.9 (C7). $[M+H]^+$ $C_{12}H_{13}N_2O$ calculated: 201.102239, $[M+H]^+$ $C_{12}H_{13}N_2O$ found: 201.102312.

2.1.7. (E)-2-(((thiophen-2-ylmethylene)amino)methyl)phenol (3f)

In a porcelain mortar 0.30 g (2.4 mmol) of 2- (hydroxymethyl) aniline and 0.27 g (2.4 mmol) of 2-thiophenecarboxaldehyde were placed, and then the general procedure was followed. A brown powder was obtained; yield 96%; mp: 83 °C; IR (ATR, cm^{-1}): 3326 (OH), 1610 (C=N), 1545 (N-H), 1485 (C=C), 1439 (C-N). ^{1}H NMR ($CDCl_3$, 500 MHz, δ): 8.54 (s, 1H, H8), 7.50-7.46 (m, 1H, H10), 7.30-7.29 (m, 1H, H12), 7.19-7.15 (m, 2H, H6, H4), 7.17-7.04 (m, 3H, H3, H5, H11), 4.76 (s, 2H, H7). ^{13}C NMR (125 MHz, $CDCl_3$) δ 152.28 (C8), 148.89 (C2), 141.09 (C9), 132.71 (C6), 131.01 (C10), 128.63 (C12), 128.34 (C4), 128.04 (C11), 126.65 (C1), 122.17 (C5), 117.38 (C3), 64.06 (C7). $[M+H]^+$ $C_{12}H_{11}NOS$ calculated: 218.06341, $[M+H]^+$ $C_{12}H_{11}NOS$ found: 218.06350.

2.1.8. Selectivity evaluation of different metals

The evaluation of imines' selectivity was carried out, preparing a solution of the imine **3a-3f** (**L**) with a concentration of 10 μM in CH_3CN. Also aqueous solutions with a concentration of 10 μM of the metals (**M**): Ba^{2+}, Co^{2+}, Fe^{2+}, Mg^{2+}, Ni^{2+}, Pb^{2+}, Zn^{2+}, Cd^{2+}, Hg^{2+}, Cu^{2+}, Sn^{2+} and Cs^+ were prepared. The selectivity was achieved by placing 1 mL of **L** in 10 different vials, and 1 mL of the metal solution was added to each one (**L+M**).

3. Results and discussion

3.1. Imines synthesis

The two components of a colorimetric organic sensor are the receptor and the transducer. The receptor is responsible for the recognition, generally through coordination, so heteroatoms with lone pair electrons can be used, such as N, S, O, P, and B. On the other hand, the transducer is responsible for converting the coordination system into a visible optical signal. In the imines, the conjugated double bond system acts as transducers. Imines are relatively easy to synthesize molecules; heteroatoms with free electron pairs allow its incorporation into a π-conjugated system, making their molecular engineering easy to manipulate. Some fragments like heterocycles rings and salicylaldehyde were included in the molecule to introduce lone pair electrons as a receptor. The synthesis of **3a-3d** imines was carried out through a condensation reaction using salicylaldehyde and the corresponding amine, as shown in Scheme 1. The 3e and 3f synthesis was carried out by the condensation of 2-amino-benzyl alcohol, with pyrrole-2-carboxaldehyde, and 2-thiophenecarboxaldehyde, respectively. Reactions were carried out using mechanochemistry at environmental conditions, in the absence of solvent at 30 °C. The yields obtained were in the range of 76-96%.

Table 1
Optical characterization of imines 3a-3f.

Comp (L)	Yield (%)	Abs (λ_{max} nm)	Eg^{op} (eV)*	Eg^{cal} (eV)++
3a	88	362	3.43	3.86
3b	86	360	3.45	3.88
3c	76	348	3.57	3.51
3d	90	370	3.35	3.97
3e	92	326	3.81	3.69
3f	96	292	4.25	3.97

* Was obtained from equation $Eg = 1243/\lambda$.
++ Obtained by calculations using DFT.

The chemical structure characterization was performed using FT-IR, 1D, and 2D NMR and mass spectrometry. In the FT-IR spectra, two characteristic bands were observed for these compounds; the first one is shifted to 3500–3244 cm^{-1} region corresponding to the O–H bond strain vibrations; this is broadband, which means that the hydroxyl hydrogen is forming a strong hydrogen bond (O–H···A). The second band observed is the corresponding to the carbon-nitrogen double bond (C = N), which was detected in 1615, 1655, 1613, 1603, 1619, and 1610 cm^{-1} for **3a, 3b, 3c, 3d, 3e,** and **3f** respectively, this signal confirms the imine formation.

^{1}H NMR corroborated the imines structures; the amino hydrogen of **3a, 3b, 3c, 3d, 3e**, and **3f**, were shifted at δ = 8.7, 8.9, 9.1, 9.4, 8.2, and 8.6 ppm, respectively. The ^{1}H spectrum integration of the signals corresponds to the total number of hydrogens in each molecule under study. On the other hand, using ^{13}C NMR, it was found that the chemical shift of the imine carbons (C = N) of **3a, 3b, 3c, 3d, 3e**, and **3f,** was 159, 166, 163, 165, 149, and 152 ppm, respectively. The imine **3a** is in equilibrium in 96:4 *cis/trans* ratio, while **3e** and **3f** are in an imine/1,3-oxazinane equilibrium. In **3e,** the equilibrium is shifted to the imine form in a 95:5 ratio. In compound **3f,** the equilibrium is in a 50:50 ratio (the ratio was established using the integrals in the ^{1}H NMR, SI spectra) (Scheme 2).

3.2. Optical properties and assessment of 3a-3f selectivity to different metals

First, the UV-Vis spectrum of **3a-3f** 10 μM was obtained; the maximum of absorption band (λ_{max}) values are shown in Table 1, where it is demonstrated that imine **3d** was the most red-shifted with a λ_{max} at 370 nm, so the compound is yellow with a band-gap of 3.35 eV. The imine **3f** presents a λ_{max} at 292 nm with the largest band-gap (4.25 eV). Subsequently, the absorption spectra of each imine with the different metals were obtained (Fig. 1). Compounds **3a, 3b, 3d,** and **3f** did not show selectivity to metals in aqueous solution. Imine **3a** is coordinated to most metals with a new band formation at 445 nm. On the other hand, the imine **3d** has photoluminescence in the presence of Pb^{2+}, Sn^{2+}, Fe^{2+}, Hg^{2+}, and Cu^{2+}, under an excitation source of 352 nm. Compound **3c** initially presented a band at 348 nm as a colorless solution, in the presence of Hg^{2+}, Ni^{2+}, and Cu^{2+}, the formation of a small band was observed at 461, 422, and 412 nm respectively, accompanied by a yellow color in solution

3.3. Metal ion interference and determination of detection limit

Finally, when compound **3e** was evaluated as a sensor to different metals, only the mixture **3e** + $\mathbf{Cu^{2+}}$, presented a change of coloration (from colorless to yellow), while the rest of the mixtures **3e+M** remained colorless. This result indicates that **3e** is a chemical sensor selective to Cu^{2+} (Fig. 1). The UV-Vis spectrum, shows that 3e absorption bands do not shift when the metals solutions of; Ba^{2+}, Co^{2+}, Fe^{2+}, Mg^{2+}, Ni^{2+}, Pb^{2+}, Zn^{2+}, Cd^{2+}, $Sn^{2+,}$ and Cs^+

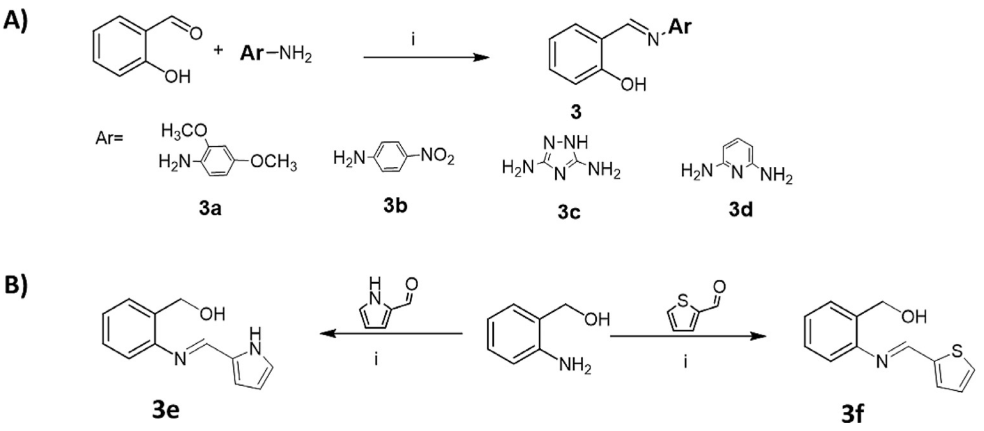

Scheme 1. Synthetic route of imines 3a-3f, i) Grinding 30 °C, 30 min, solvent-free.

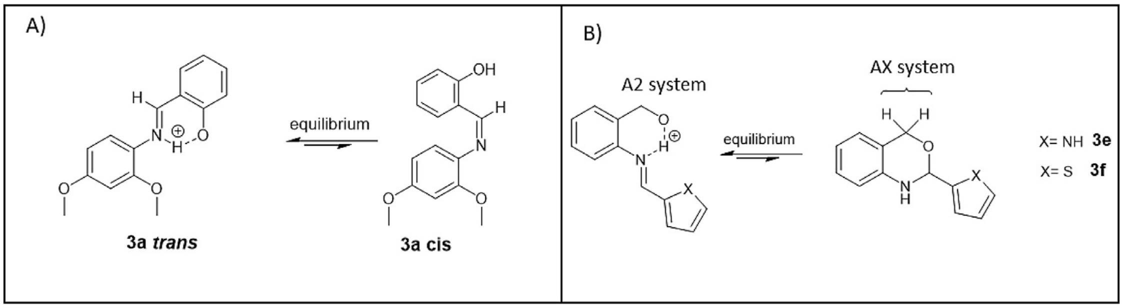

Scheme 2. Chemical equilibrium A) *cis–trans* isomerization of 3a, B) Imine – 1,3-oxazinane equilibrium for 3e and 3f.

are added, except when Hg^{2+} is used since the maximum absorption band of **3e** is shifted to the infrared at 342 nm, without a change in the solution color. On the other hand, when Cu^{2+} solution is added, a band formation at 406 nm is observed, attributed to the coordination of **3e** with Cu^{2+}, forming an internal charge transfer complex (ICT). The ICT, causes an electronic density redistribution of the π-conjugate system and energy-gap reduction (Eg), causing a band redshift and the yellow solution coloration.

Usually, the water sources could contain more than one metal; thus, it was performed an interference test of metal ions using the compound **3e** as a sensor. For this purpose, three different solutions were prepared. The first solution contains the metals; Ba^{2+}, Co^{2+}, Fe^{2+}, Mg^{2+}, Ni^{2+}, Pb^{2+}, Zn^{2+}, and Cd^{2+} (**L+M**), the second have the same metals, including Hg^{2+} (**L+ M+Hg^{2+}**), and the third one includes the metals of **L+ M** more Cu^{2+} (**L+ M+Cu^{2+}**). Then the sensor **3e** (**L**) was mixed with the aqueous solution **S1**, where no color change was observed, and the band at 326 nm of L did not change. On the other hand, when the solution **S3** containing Cu^{2+} was mixed with **3e**, the solution turned colorless to yellow, which indicates that there is no interference from other metals present that prevent the detection of Cu^{2+} by the sensor **3e** (Fig. 2).

3.4. Determination of the association constant (K_a)

The titration of **3e**, dissolved in ACN, was carried out using an aqueous solution of Cu^{2+}, which allowed to determine the association constant (Ka) of the **L+Cu^{2+}** complex and the sensor sensitivity. The titration was carried out in a range of 0.04 to 3 equivalents of Cu^{2+} concerning **3e**. During the titration process, two bands absorption were monitored mainly, the first band corresponding to the L sensor at 326 nm, the second band at 406 nm, which corresponds to the **L+Cu^{2+}** complex. As the Cu^{2+} solution is added, the band intensity at 326 nm decreases, while the band intensity of the **L+Cu^{2+}** increases; this phenomenon occurs until reaching an **L:Cu^{2+}** equivalence of 1:1; subsequently, the intensity of the bands do not change considerably (Figure 3). The presence of an isosbestic point at 352 nm suggests that there is just one specie in equilibrium between L free and the complex **L+Cu^{2+}**. The association constant (Ka) to form **L+Cu^{2+}** was determined using the Benesi-Hildebrand equation (Eq. 1).

$$\frac{1}{A-A_0}=\frac{1}{K_a(A_{\max}-A_0)[\mathrm{Cu2+}]}+\frac{1}{A_{\max}-A_0} \quad (1)$$

Where **A** represents the absorbance of L when different amounts of Cu^{2+} are added, $\mathbf{A_0}$ is the absorbance of **L** in the absence of Cu^{2+}. $\mathbf{A_{max}}$ represents the absorbance of L in the presence of an excess of Cu^{2+}. **[Cu^{2+}]** is the concentration of metal added during the titration. The term **[1/(A-A0)]** varies as a function of **1/[Cu^{2+}]** in a linear form with a value of R = 0.983. Using the Eq. 1 association constant of **L+Cu^{2+}** in acetonitrile was determined to be 8.24×10^3 M^{-1}

Through the titration, it was also possible to determine the detection limit of L; first, visually, the color change from colorless to yellow can be perceived with a metal concentration of 1.4×10^{-5} M, while using a UV-Vis equipment, it can be detected up to 4.9×10^{-6} M.

The imine **3e** was titrated using a solution of Cu^{2+} to generate the Jobś plot, which is shown in Fig. 3b. The lines in the Job's plot are intersected when the mole fraction of Cu^{2+} is 0.5; this indicates that the complex formed between the imine and metal ion has a 1:1 stoichiometry.

Table 2 shows some imines that have been evaluated as metal ion sensors in previously reported works. First, it is observed that imines tend to act as colorimetric and fluorescent sensors selective to Ni2+ and Cu2+. Compared to other organic sensors, imines can detect very low concentrations of metals in aqueous media. For this reason, they are considered among the most sensitive organic sensors. Of the imines compared, 3e is the one with the lowest de-

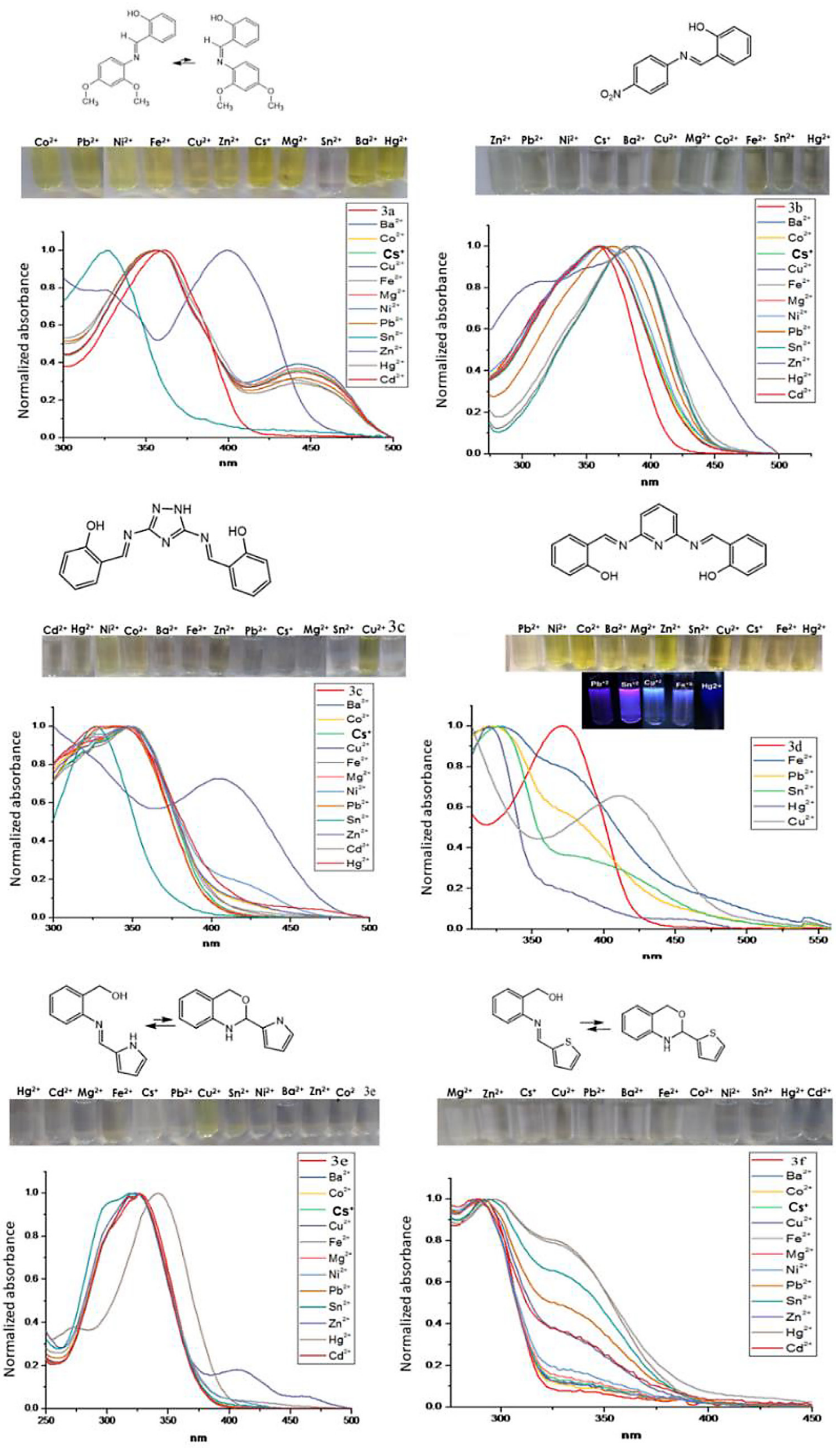

Fig. 1. A) Colorimetric test of selectivity in solution (CH_3CN/Water) of ligands 3a-3f with different metal ions. B) UV-Vis absorption spectrum of the L+M mixture (1: 1).

Table 2
Comparison of LOD for different Schiff bases.

Schiff base	Detection method	Selectivity	Binding constant [M^{-1}]	Detection limit	Ref.
5-Chloro-2-[(1E,2E)-3-(4-(dimethylamino) phenyl)-allyidene)amino]phenol	Colorimetric	Cu^{2+}	1.0×10^6	0.12 µM	[35]
Schiff base **L**	Fluorescent	Cu^{2+}	2.84×10^5	1.54×10^{-9} M	[32]
Schiff base **L**	Colorimetric	Ni^{2+}	ND	ND	[31]
2-((5-methylpyridin-2-ylimino)methyl)phenol	Colorimetric	Ni^{2+} and Zn^{2+}	2.09×10^4 and 5.64×10^4	6.96×10^{-7}M and 4.17×10^{-7}M	[39]
Schiff base **PN**	Fluorescent and Colorimetric	Cu^{2+}	4.489×10^4	0.179 μM.	[40]
Schiff base **3e**	Colorimetric	Cu^{2+}	8.24×10^3	4.9×10^{-6} M	This work

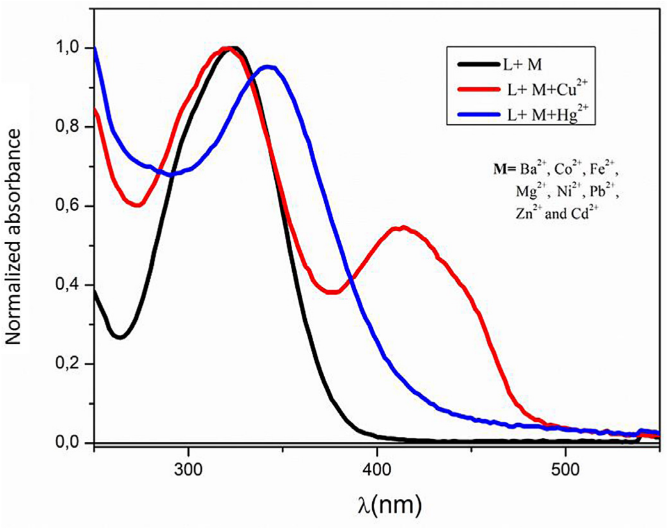

Fig. 2. Assessment of metallic ion interference in the Cu^{2+} detection.

tection limit (4.9 × 10-6 M), while the one with the highest LOD was the L-base Schiff (1.54 × 10−9 M). However, the way of detection is by fluorescence. Imine has the advantage that it is a colorimetric sensor that can be distinguished by the human eye, while for fluorescence, an excitation source is required.

3.5. Structure determination of the complex L+Cu^{2+} formed

The titration of 3e with metal established that the stoichiometry ratio between the **3e** and Cu^{2+} is 1:1. However, the possibilities of coordination between the metal and L are varied. **L** has three heteroatoms with lone pairs of electrons, so it is essential to determine the coordination complex structure. This information is relevant to establish a relationship between the ligand and metal, also be able to design sensors to be more efficient. The infrared spectrum of L in solid-state was obtained to determine the structure of the **L+M** complex. The complex **3e+Cu^{2+}** sample was prepared by mechanosynthesis; in a mortar, a 1:1 mixture of the sensor and $Cu(ClO_4)_2{\cdot}6H_2O$, was ground for five minutes. A yellow powder was obtained and analyzed by IR spectroscopy (both spectra are shown in Fig. 4).

In the IR spectrum, the free ligand presents a sharp band at 3403 cm^{-1}, for the N–H vibration bond of pyrrole ring, a broad signal at 3364 cm^{-1} correspondings to the O–H bond, the shape of the signal is known to be forming strong hydrogen bonding (this type of imines forms hydrogen bonds O–H···N) [41,42]. Finally, a band at 1619 cm^{-1} is observed, which corresponding to

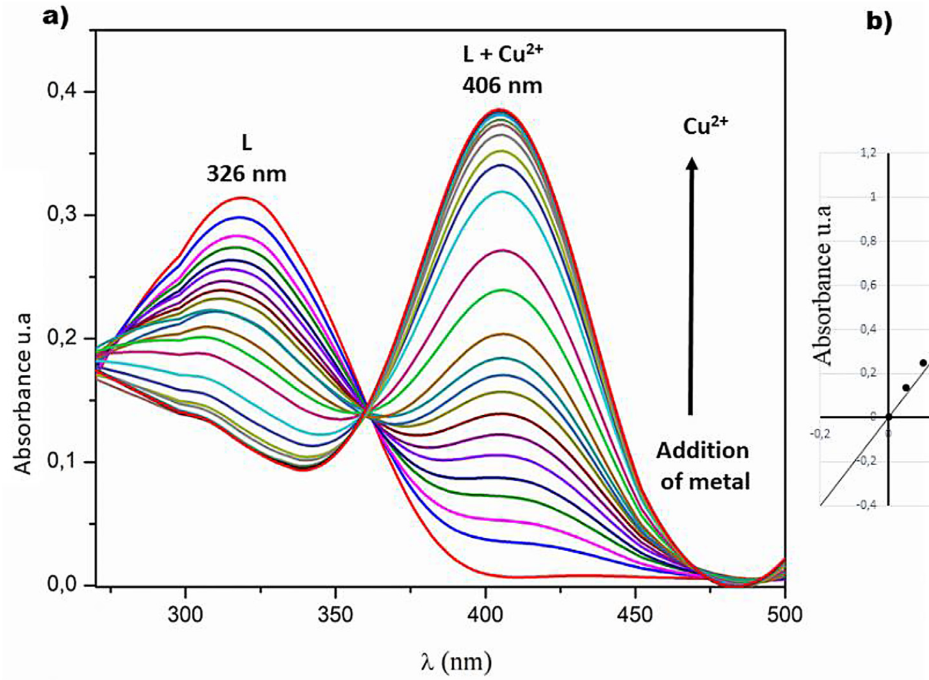

Fig. 3. a) UV absorption spectra of 3e titration using Cu^{2+} in water in different concentrations and determination of association constant (8.24×10^3 M^{-1}) and detection limit (4.9×10^{-6} M) of 3e. b) Titration to obtain the Job's plot to determine the L+M stoichiometry (1:1), the absorbance was measured at 406 nm.

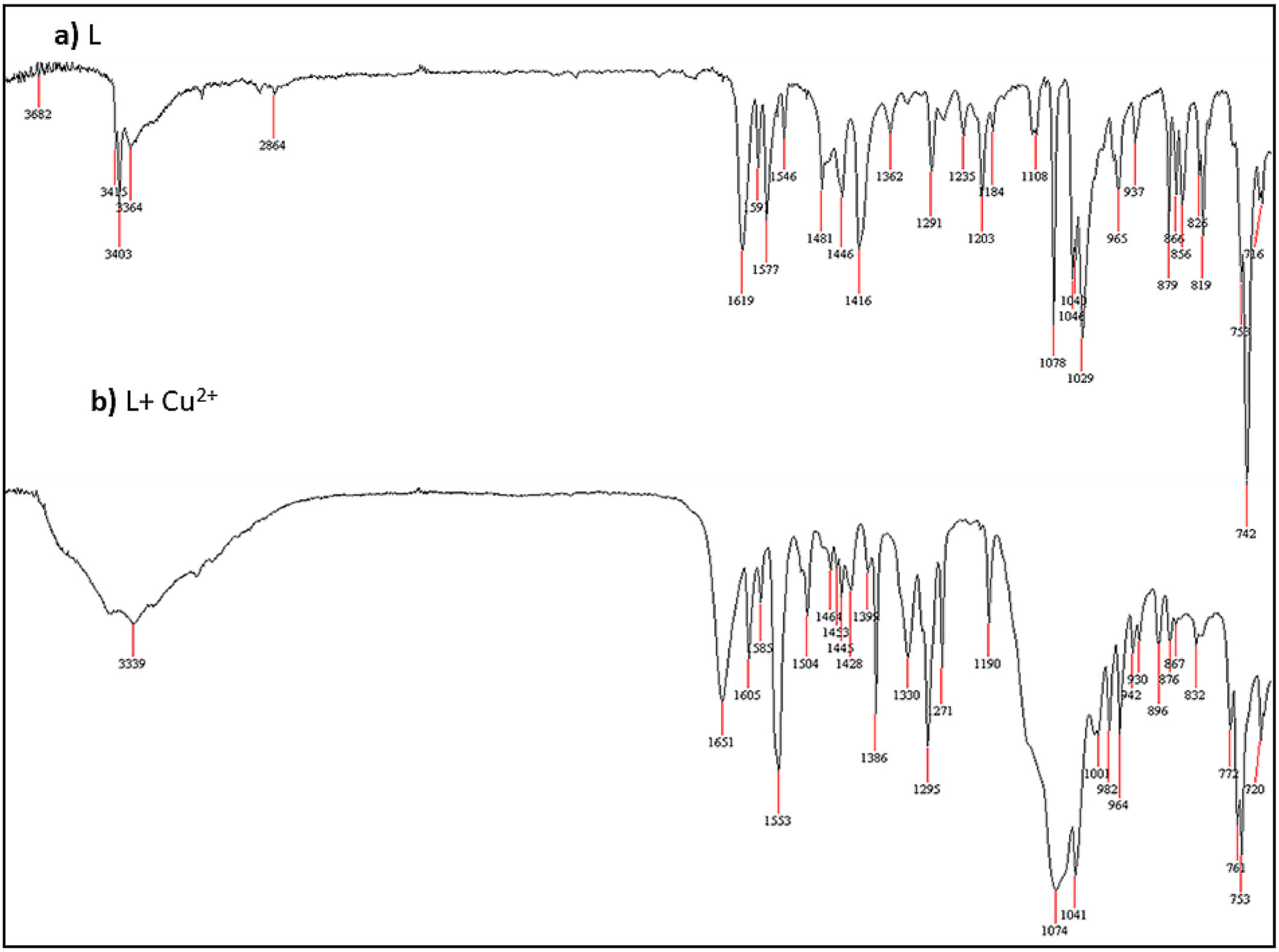

Fig. 4. IR spectra obtained by ATR. a) IR spectrum of 3e in solid state. b) IR spectrum of the metal complex 3e+Cu^{2+} in solid state.

the C=N vibrational bond. On the other hand, a wideband ranging from 3668 to 2908 cm^{-1} is observed, which does not allow the identification of N–H and O–H signals. This band is maybe due to the water presence, and it is attributed to a strong hydrogen bonding. Also, the band corresponding to the C=N bond was shifted to higher frequencies at 1651 cm^{-1}, which is indicative of the formation of the complex, very possibly through the free pair of nitrogen ($nN \longrightarrow Cu^{2+}$).

Since IR data was not plausible to determine the OH and NH role in the coordination of the metal, ^1H NMR spectroscopy was used. However, because Cu^{2+} is a paramagnetic compound, the metal was substituted by $AlCl_3$ salt, which can be coordinated to L and does not intervene in obtaining the spectra (Fig. 5). The complex was prepared by placing equivalent amounts of **L** and metal (1:1) in a mortar. The mixture was ground in the absence of a solvent for 5 min. Subsequently, 50 mg was taken, and $CDCl_3$ was added. The ^1H NMR spectrum was obtained and compared with the free binder (Fig. 5).

The ^1H NMR spectrum of **3e** shows an equilibrium between the imine and its closed-form in a 95:5 ratio. The imine hydrogen (H8) in **3e** is shifted to 8.2 ppm while H7 at 4.8 ppm. The hydrogens corresponding to the pyrrole H12, H11, and H10 are found at 6.7, 6.3, and 6.9 ppm, respectively. Finally, the O-H hydrogen is observed at 10.61 ppm, which is not exchanged with D, since it forms a strong hydrogen bond (O–H···N, Fig. 5). On the other hand, the spectrum of **3e+Al^{3+}** shows that when coordination is carried out, the most affected hydrogens are H8, which corresponds to the imine hydrogen, it is shifted at 9.14 ppm ($\Delta\delta = 0.94$), H12 is shifted to 7.0 ppm ($\Delta\delta = 0.3$), H11 was virtually unaffected. In comparison, H10 is shifted to a higher frequency (7.06 ppm, $\Delta\delta = 0.16$). As the H8 signal disappeared, so the hydrogen bond (O–H···N) is not forming. We propose that the metal coordinates with the three heteroatoms present in the molecule based on this information.

3.6. Computational analysis

To find the relationship between the molecule chemical structure and metal selectivity, the geometry, electronic distribution, and HOMO-LUMO energy levels position were studied. Computational calculations were performed using density functional theory (DFT). The geometries were optimized using Gaussian 09 software [43], using the B3LYP functional [44]. The geometry, as well as the energies of the HOMO-LUMO orbitals, are shown in Fig. 6. According to the geometry in all the molecules, the nitrogen is in the same plane as the OH, forming hydrogen bonds O–H···N, corroborated by ^1H NMR. Furthermore, the electronic distribution in all cases was found throughout the π-conjugate system.

The molecule geometry could determine the ligand coordination with the metal since the lone pair electrons of the heteroatoms must be arranged to coordinate. Considering the geometry determined by DFT, both the nitrogen lone pair electron and

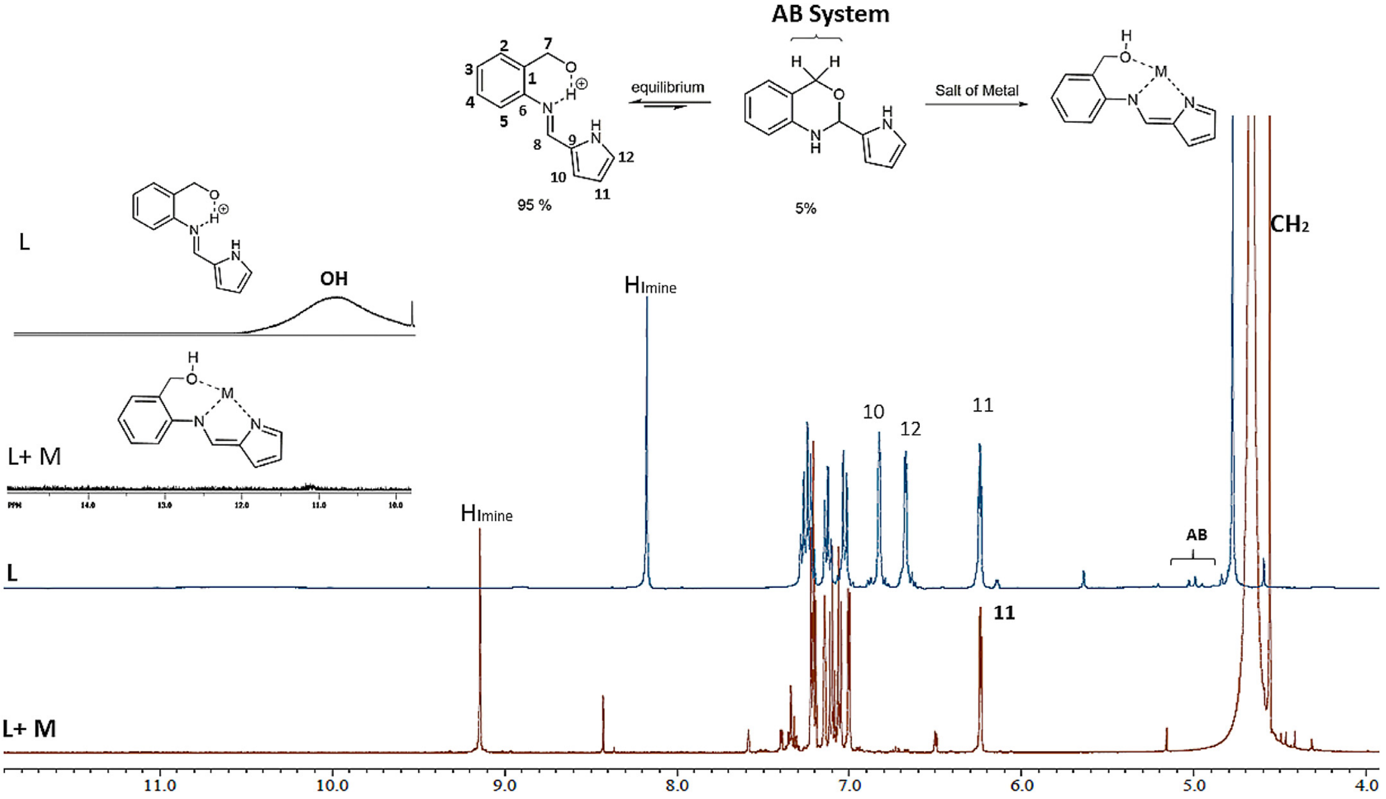

Fig. 5. ^{1}H NMR spectrum of 3e (blue) and ^{1}H NMR spectrum of 3e+M (red). Comparison of chemical shifts. Both samples were prepared taking 50 mg and dissolved in 1 mL of $CDCl_3$.

Table 3
Electronic transition and the electronic parameters of molecular orbitals involved.

	HOMO/LUMO Eg (eV)	Osc. Strength	Transition
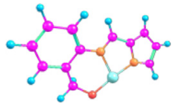 **L+M**	-5.44/-2.77 2.67	0.0019	H-6(B) →LUMO(B) (66%) H-5(B) →LUMO(B) (10%)
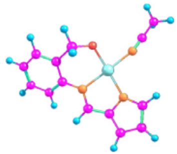 **L+M.ACN**	-4.91/-2.36 2.55	0.0009	H-9(B) → LUMO(B) (11%) H-7(B) → LUMO(B) (11%) H-6(B) → LUMO(B) (22%) HOMO(B)→ LUMO(B) (21%)
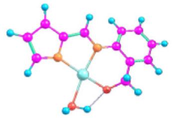 **L+M.H_2O**	-5.25/-2.77 2.48	0.0004	HOMO(A)→ LUMO(A) (48%) HOMO(B) → L+1(B) (49%)

the OH group of alcohol are oriented on the same side for 3a-3d, thus promoting This allows the N ⋯ H-O bond. However, for **3e-f**, the OH group deviates from the plane, explaining the equilibrium between the imine and the six-membered cycle observed by NMR. In the 3e-f open form, the lone pair electrons of the heteroatoms are free to coordinate the metal, although only compound 3e coordinates the copper whit a color change.

HOMO-LUMO orbitals energies were calculated using DFT and band-gap energy (Eg = HOMO - LUMO) for 3a-3f. For compound 3a, the HOMO energy was -5.23 eV and LUMO of -1.36 eV with Eg = 3.86 eV, for 3b the HOMO was -6.44 eV and LUMO of -2.56 eV with Eg = 3.88 eV, for the compound 3c the HOMO = -5.81 eV and the LUMO = -2.29 eV, for 3d the energy of HOMO = -5.90 eV and LUMO = -1.92 eV with an Eg = 3.97 eV, for the compound 3e, HOMO = -5.46 and LUMO = -1.77 eV, with an Eg = 3.69, finally for 3f, the energy of HOMO = -5.98 eV and LUMO = -2.01 eV, with an Eg = 3.97 eV. The Eg energy calculated by DFT is closely correlated with those determined experimentally (Fig. 6). The Eg energy of the imines is very close to each other. However, the HOMO orbital position varies and could be responsible for the selectivity of imine 3e.

As the lone pair electrons of **3a-3f** are involved in the metal coordination, the HOMO orbital of the Schiff base must be decisive to form the L + M complex and could be involved in selectivity. Figure 7 shows the HOMO energy positions of the imines. In this, it can be seen that HOMO energy values for **3a** and **3e** were -

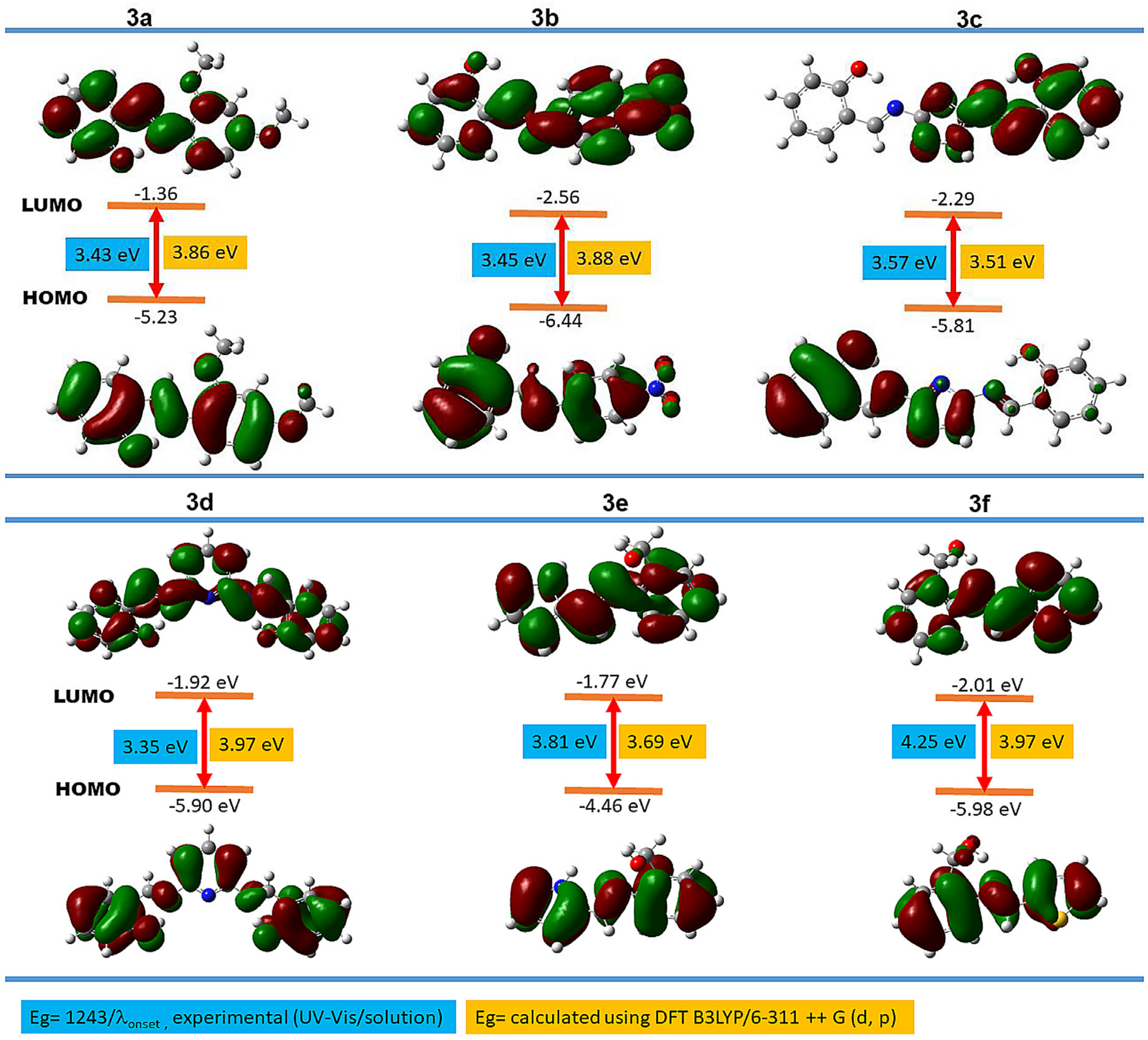

Fig. 6. Geometries optimization of 3a-3f, electronic density distribution, as well as HOMO-LUMO energies, using DFT at B3LYP/6-311 ++G level.

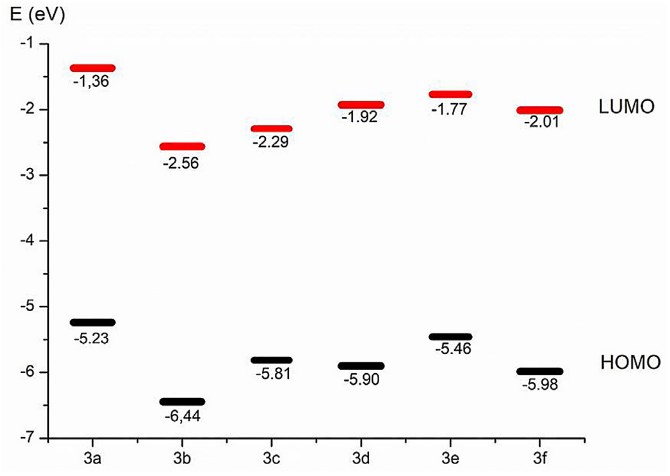

Fig. 7. Comparison and position of HOMO-LUMO energy levels of 3a-3f.

5.23 and -5.46 eV, respectively. The compound 3a was coordinated with most metals in the selectivity test, while compound **3e** was selective to Cu^{2+}. For compounds **3b, 3c, 3d**, and **3f**, the energy of the HOMO orbital are below -5.8 eV, suggesting that molecules designed as sensors of metal ions of Hg^{2+}, Cu^{2+}, Zn^{2+}, Fe^{2+}, Mn^{2+}, Co^{2+}, Pb^{2+}, and Cd^{2+}, the energy of the HOMO orbital must be between -5.23 and -5.46 eV.

To determine the L+M complex of **3e** with Cu^{2+} calculation using the base 6-311 ++ G (d, p) was carried out for systems containing C, H, N, and O [45], for the Cu^{2+} LANL2DZ basis sets was used. A frequency analysis was carried out for all optimized geometries to ensure that they are not imaginary states. As a result, three possible coordination complexes were obtained, which are agree with NMR and IR data (Fig. 8). In the first complex, Cu^{2+} atom is coordinated to both nitrogens and the oxygen in **3e,** (Excitation parameters obtained for the Td-DFT studies of the complex are shown in Table 3). The second complex proposed is the coordination of Cu^{2+} with the three heteroatoms in **3e** and a molecule of solvent (ACN); however, the new band formed is shifted to 600 nm. In the third complex, the structure proposed the molecule ACN is changed by H_2O. In this complex, a new band is observed at 584 nm. The HOMO and LUMO energies are shown in Fig. 8, showing the electronic density distribution and the band-gap energy obtained.

The energy Eg of the calculated complexes was determined by using the Eg = HOMO-LUMO equation. Experimentally the band-gap of **3e+Cu^{2+}** (Eg = 3.06 eV) was determined using the equation E = hν (1243 / λ_{onset}). According to the data calculated from the electronic transitions obtained by TD-DFT, the complex most

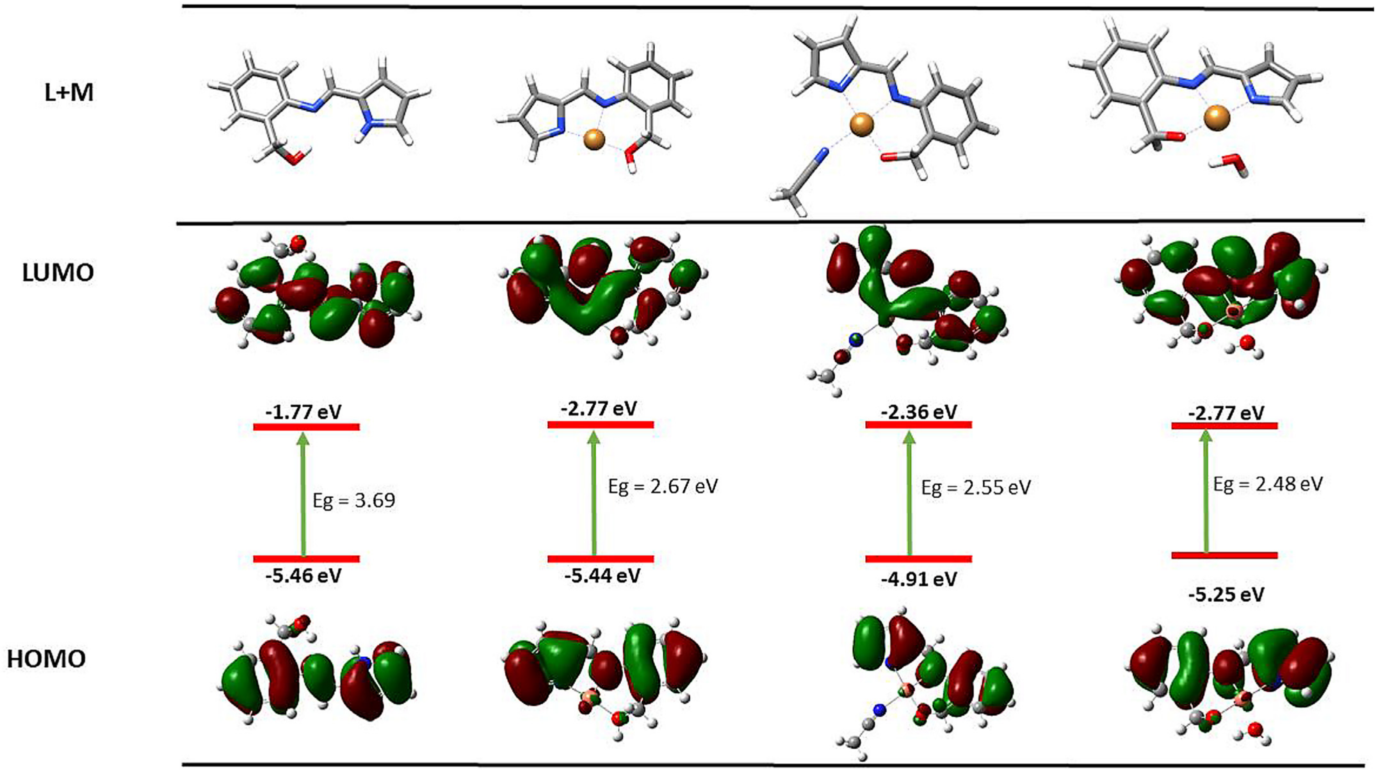

Fig. 8. Geometries optimization of L and L+Cu^{2+} complex, determination of the electronic density distribution, as well as HOMO-LUMO energies, by using DFT.

closely matches the experimental parameters is when 3e coordinates with both nitrogens and oxygen at the same time to Cu^{2+}. Of the three proposed structures, **L+M** is the closest to the experimental value (Eg cal = 2.67 eV). The energy of the complexes **L+M.ACN** and **L+M.H$_2$O** are not consistent with the experimental result, with Eg= 2.55, and Eg=2.48 eV. Finally, it can be seen that in the L+M complex, the electron density distribution in the HOMO orbital is delocalized along with the π-conjugate system. In contrast, in the LUMO orbital, it is located over the Cu^{2+} and pyrrole ring; it is a complex with ICT, responsible for the coloration change from colorless to yellow.

4. Conclusion

The solvent-free synthesis of six imines through mechanochemistry and their structural characterization was carried out. The imines **3a-3f** were evaluated as chemical sensors for heavy metals detection in an aqueous medium. **3e** was a selective colorimetric sensor to Cu^{2+} even in the presence of others metal ions such as Ba^{2+}, Co^{2+}, Fe^{2+}, Mg^{2+}, Ni^{2+}, Pb^{2+}, Zn^{2+}, Hg^{2+}, and Cd^{2+}. The sensor has a detection limit to the naked eye (by color change) of 2.49×10^{-5} M, while with the use of UV-Vis equipment, it was 4.9×10^{-6} M. The association constant Ka of **3e+Cu^{2+}** was determined to be 8.246×10^{3} M^{-1}. Through IR, ^{1}H NMR, and DFT calculations, it was found that complex is formed by a molecule of **3e** and a Cu^{2+} atom and that the three heteroatoms present in the molecule coordinate the metal.

On the other hand, it was determined that the absorption band shifted from 326 to 406 nm is due to electron density redistribution of L in the complex formation, since an internal charge transfer complex is formed in the coordination. The relationship between the coordination with metals and the HOMO energy levels suggests a trend in the selectivity of organic sensors, where the HOMO of the organic molecule controls the selectivity to metals. This information is relevant since molecular engineering allows modulating the energy levels by introducing electron-withdrawing and donating groups to design intelligent organic sensors.

Credit Author Statement

Cesar Garcias and Josue Maldonado carried out the design, synthesis, and characterization of the reported molecules. Also, C.G supervised the project implementation and performed the data analysis. Armando Ariza carried out the IR experiments, High-resolution mass band NMR caracterization. A.E.-R. Performed the theoretical calculations. Catalina M. Perez, Marco Lobato, and Mario Rodriguez carried out the optical characterization, sensors evaluation, and titrations. All authors participated in the writing and editing of this article.

Declaration of Competing Interest

The authors declare that they have no known competing financial interests or personal relationships that could have appeared to influence the work reported in this paper.

Acknowledgments

Thanks to Secretary of Public Education SEP, the program supports incorporating new full-time professors (UACOAH-PTC-450) for the financing granted. To Ricardo Sebastián Mirón, Susana Lucia Estrada, and Jorge Camacho Ruiz, for the laboratory support and Cortez Picasso Ma. Teresa, for the support provided in NMR.

Supplementary materials

Experimental ^{1}H, ^{13}C-NMR, and IR spectrum for **3e-3f** can be consulted in the supporting information. Supplementary material associated with this article can be found, in the online version, at doi:10.1016/j.molstruc.2020.129444.

References

[1] D. Wu, A.C. Sedgwick, T. Gunnlaugsson, E.U. Akkaya, J. Yoon, T.D. James, Fluorescent chemosensors: the past, present and future, Chem. Soc. Rev. 46 (2017) 7105–7123, doi:10.1039/c7cs00240h.

[2] L. He, B. Dong, Y. Liu, W. Lin, Fluorescent chemosensors manipulated by dual/triple interplaying sensing mechanisms, Chem. Soc. Rev. 45 (2016) 6449–6461, doi:10.1039/c6cs00413j.

[3] X. Zhou, S. Lee, Z. Xu, J. Yoon, Recent progress on the development of chemosensors for gases, Chem. Rev. 115 (2015) 7944–8000, doi:10.1021/cr500567r.

[4] Y. Salinas, R. Martínez-Máñez, M.D. Marcos, F. Sancenón, A.M. Costero, M. Parra, S. Gil, Optical chemosensors and reagents to detect explosives, Chem. Soc. Rev. 41 (2012) 1261–1296, doi:10.1039/c1cs15173h.

[5] M.E. Germain, M.J. Knapp, Optical explosives detection: From color changes to fluorescence turn-on, Chem. Soc. Rev. 38 (2009) 2543–2555, doi:10.1039/b809631g.

[6] M. Kose, H. Kırpık, A. Kose, Fluorimetric detections of nitroaromatic explosives by polyaromatic imine conjugates, J. Mol. Struct. 1185 (2019) 369–378, doi:10.1016/j.molstruc.2019.03.003.

[7] K. Kopra, V. Eskonen, T. Seppälä, J. Jakovleva, R. Huttunen, H. Härmä, Peptic Fluorescent “Signal-On” and “Signal-Off” sensors utilized for the detection protein post-translational modifications, ACS Omega 4 (2019) 4269–4275, doi:10.1021/acsomega.8b03672.

[8] X. Li, C. Cao, P. Wei, M. Xu, Z. Liu, L. Liu, Y. Zhong, R. Li, Y. Zhou, T. Yi, Self-assembly of amphiphilic peptides for recognizing high furin- expressing cancer cells, (2019). doi:10.1021/acsami.9b01281.

[9] R.J. Soto, J.R. Hall, M.D. Brown, J.B. Taylor, M.H. Schoenfisch, In Vivo Chemical Sensors, Role of biocompatibility on performance and utility, Anal. Chem. 89 (2017) 276–299, doi:10.1021/acs.analchem.6b04251.

[10] Y. Zhang, S. Luo, Y. Tang, L. Yu, K. Hou, J. Cheng, X. Zeng, P.G. Wang, Carbohydrate - protein interactions by “ Clicked ” carbohydrate self-assembled monolayers, 78 (2008) 2001–2008.

[11] F.Y. Yi, D. Chen, M.K. Wu, L. Han, H.L. Jiang, Chemical sensors based on metal–organic frameworks, Chempluschem 81 (2016) 675–690, doi:10.1002/cplu.201600137.

[12] H. Zhu, J. Fan, B. Wang, X. Peng, MRI Fluorescent, and colorimetric chemical sensors for the first-row d-block metal ions, Chem. Soc. Rev. 44 (2015) 4337–4366, doi:10.1039/c4cs00285g.

[13] H.N. Kim, W.X. Ren, J.S. Kim, J. Yoon, Fluorescent and colorimetric sensors for detection of lead, cadmium, and mercury ions, Chem. Soc. Rev. 41 (2012) 3210–3244, doi:10.1039/c1cs15245a.

[14] A.J. Bandodkar, I. Jeerapan, J. Wang, Wearable chemical sensors: present challenges and future prospects, ACS Sensors 1 (2016) 464–482, doi:10.1021/acssensors.6b00250.

[15] M.R. Hopkins, A.S. Ettinger, M. Hernández-Avilla, J. Schwartz, M.M. Téllez-Rajo, H. Lamadrid-Figueroa, D. Bellinger, H. Hu, R.O. Wright, Variants in iron metabolism genes predict higher blood lead levels in young children, Environ. Health Perspect. 116 (2008) 1261–1266, doi:10.1289/ehp.11233.

[16] C.N. McFarland, L.I. Bendell-Young, C. Guglielmo, T.D. Williams, Kidney, liver and bone cadmium content in the western sandpiper in relation to migration, J. Environ. Monit. 4 (2002) 791–795, doi:10.1039/b206045k.

[17] T.W. Clarkson, L. Magos, G.J. Myers, The toxicology of mercury — current exposures and clinical manifestations, N. Engl. J. Med. 349 (2003) 1731–1737, doi:10.1056/NEJMra022471.

[18] C.M.L. Carvalho, E.H. Chew, S.I. Hashemy, J. Lu, A. Holmgren, Inhibition of the human thioredoxin system: a molecular mechanism of mercury toxicity, J. Biol. Chem. 283 (2008) 11913–11923, doi:10.1074/jbc.M710133200.

[19] X. Sun, Y. Wang, Y. Lei, Fluorescence based explosive detection: from mechanisms to sensory materials, Chem. Soc. Rev. 44 (2015) 8019–8061, doi:10.1039/c5cs00496a.

[20] R. Martínez, A. Espinosa, A. Tárraga, P. Molina, A new bis(pyrenyl)azadiene-based probe for the colorimetric and fluorescent sensing of Cu(II) and Hg(II), Tetrahedron 66 (2010) 3662–3667, doi:10.1016/j.tet.2010.03.080.

[21] I.T. Ho, G.H. Lee, W.S. Chung, Synthesis of upper-rim allyl- and p-methoxyphenylazocalix[4]arenes and their efficiencies in chromogenic sensing of Hg^{2+} ion, J. Org. Chem. 72 (2007) 2434–2442, doi:10.1021/jo062280s.

[22] P. Saluja, H. Sharma, N. Kaur, N. Singh, D.O. Jang, Benzimidazole-based imine-linked chemosensor: chromogenic sensor for Mg^{2+} and fluorescent sensor for Cr^{3+}, Tetrahedron 68 (2012) 2289–2293, doi:10.1016/j.tet.2012.01.047.

[23] V.K. Gupta, N. Mergu, L.K. Kumawat, A.K. Singh, A reversible fluorescence “off-on-off” sensor for sequential detection of aluminum and acetate/fluoride ions, Talanta 144 (2015) 80–89, doi:10.1016/j.talanta.2015.05.053.

[24] J.W. Jeong, B.A. Rao, J.Y. Lee, J.Y. Hwang, Y.A. Son, An “OFF-ON” fluorescent chemosensor based on rhodamine 6G-2-chloronicotinaldehyde for the detection of Al^{3+} ions: part ii, sensors actuators, B Chem. 227 (2016) 227–241, doi:10.1016/j.snb.2015.12.015.

[25] Y.S. Zhang, R. Balamurugan, J.C. Lin, S. Fitriyani, J.H. Liu, A. Emelyanenko, Pd^{2+} fluorescent sensors based on amino and imino derivatives of rhodamine and improvement of water solubility by the formation of inclusion complexes with β-cyclodextrin, Analyst 142 (2017) 1536–1544, doi:10.1039/c6an02594c.

[26] M. Chae, J. Yoon, A.W. Czarnik, Chelation-enhanced fluorescence chemosensing of Pb(II), an inherently quenching metal ion, J. Mol. Recognit. 9 (2002) 297–303, doi:10.1002/(sici)1099-1352(199607)9:4Glt;297::aid-jmr335⟩3.3.co;2-y.

[27] J.Y. Kwon, Y.J. Jang, Y.J. Lee, K.M. Kim, M.S. Seo, W. Nam, J. Yoon, A highly selective fluorescent chemosensor for Pb^{2+}, J. Am. Chem. Soc. 127 (2005) 10107–10111, doi:10.1021/ja051075b.

[28] A.Y. Mironenko, M.V. Tutov, A.A. Sergeev, S.Y.Bratskaya Voznesenskiy, On/off rhodamine based fluorescent probe for detection of Au and Pd in aqueous solutions, Sensors Actuators, B Chem. 246 (2017) 389–394, doi:10.1016/j.snb.2017.02.092.

[29] W. Lin, L. Yuan, X. Cao, W. Tan, Y. Feng, A coumarin-based chromogenic sensor for transition-metal ions showing ion-dependent bathochromic shift, Eur. J. Org. Chem. (2008) 4981–4987, doi:10.1002/ejoc.200800667.

[30] H.C. Erythropel, J.B. Zimmerman, T.M. De Winter, L. Petitjean, F. Melnikov, C.H. Lam, A.W. Lounsbury, K.E. Mellor, N.Z. Janković, Q. Tu, L.N. Pincus, M.M. Falinski, W. Shi, P. Coish, D.L. Plata, P.T. Anastas, The Green ChemisTREE: 20 years after taking root with the 12 principles, Green Chem. 20 (2018) 1929–1961, doi:10.1039/c8gc00482j.

[31] L. Wang, D. Ye, D. Cao, A novel coumarin Schiff-base as a Ni(II) ion colorimetric sensor, Spectrochim. Acta - Part A Mol. Biomol. Spectrosc. 90 (2012) 40–44, doi:10.1016/j.saa.2012.01.017.

[32] F. Nouri Moghadam, M. Amirnasr, S. Meghdadi, K. Eskandari, A. Buchholz, W. Plass, A new fluorene derived Schiff-base as a dual selective fluorescent probe for Cu^{2+} and CN−, Spectrochim. Acta - Part A Mol. Biomol. Spectrosc. 207 (2019) 6–15, doi:10.1016/j.saa.2018.08.058.

[33] N. Kaur, B. Kaur, Spectral studies on anthracene based dual sensor for Hg^{2+} and Al^{3+} ions with two distinct output modes of detection, Spectrochim. Acta - Part A Mol. Biomol. Spectrosc. 181 (2017) 60–64, doi:10.1016/j.saa.2017.03.029.

[34] Y.L. Leng, J.H. Zhang, Q. Li, Y.M. Zhang, Q. Lin, H. Yao, T.B. Wei, An easy prepared dual-channel chemosensor for selective and instant detection of fluoride based on double Schiff-base, Spectrochim. Acta - Part A Mol. Biomol. Spectrosc. 167 (2016) 116–121, doi:10.1016/j.saa.2016.05.040.

[35] D. Peralta-Domínguez, M. Rodriguez, G. Ramos-Ortiz, J.L. Maldonado, D. Luna-Moreno, M. Ortiz-Gutierrez, V. Barba, A Schiff base derivative used as sensor of copper through colorimetric and surface plasmon resonance techniques, sensors actuators, B Chem. 225 (2016) 221–227, doi:10.1016/j.snb.2015.11.013.

[36] D. Peralta-Domínguez, M. Rodríguez, G. Ramos-Ortíz, J.L. Maldonado, M.A. Meneses-Nava, O. Barbosa-García, R. Santillan, N. Farfán, A Schiff base derivative from cinnamaldehyde for colorimetric detection of Ni^{2+} in water, Sensors Actuators, B Chem. 207 (2015) 511–517, doi:10.1016/j.snb.2014.09.100.

[37] Y.H. Hung, A.I. Bush, R.A. Cherny, Copper in the brain and Alzheimer’s disease, J. Biol. Inorg. Chem. 15 (2010) 61–76, doi:10.1007/s00775-009-0600-y.

[38] J.C. Lee, H.B. Gray, J.R. Winkler, Copper (II) Binding to r -Synuclein, the Parkinson ’ s Protein, (2008) 6898–6899.

[39] F. Abebe, J. Gonzalez, K. Makins-Dennis, R. Shaw, A new bis(rhodamine)-based colorimetric chemosensor for Cu^{2+}, Inorg. Chem. Commun. 120 (2020) 108154, doi:10.1016/j.inoche.2020.108154.

[40] J. Wang, Q. Niu, T. Wei, T. Li, T. Hu, J. Chen, X. Qin, Q. Yang, L. Yang, Novel phenothiazine-based fast-responsive colori/fluorimetric sensor for highly sensitive, selective and reversible detection of Cu^{2+} in real water samples and its application as an efficient solid-state sensor, Microchem. J. 157 (2020) 104990, doi:10.1016/j.microc.2020.104990.

[41] D. Ortegon-Reyna, C. Garcias-Morales, E.V. García-Báez, A. Ariza-Castolo, F.J. Martínez-Martínez, (*E*)-4-Hydroxy-2-{[(2-phenylethyl)iminiumyl]methyl}phenolate, Acta Crystallogr. Sect. E Struct. Reports Online. 68 (2012) o2075–o2075, doi:10.1107/S1600536812025408.

[42] F. Martínez-Martínez, C. Garcías-Morales, A. Aríza-Castolo, I. Padilla-Martínez, A. Peraza-Campos, D. Ortegón-Reyna, E. García-Báez, NMR structural study of the prototropic equilibrium in solution of Schiff bases as model compounds, Molecules 19 (2013) 459–481, doi:10.3390/molecules19010459.

[43] M.J. Frisch, G.W. Trucks, H.B. Schlegel, G.E. Scuseria, M.A. Robb, J.R. Cheeseman, G. Scalmani, V. Barone, B. Mennucci, G.A. Petersson, H. Nakatsuji, M. Caricato, X. Li, H.P. Hratchian, A.F. Izmaylov, J. Bloino, G. Zheng, J.L. Sonnenberg, M. Hada, M. Ehara, K. Toyota, R. Fukuda, J. Hasegawa, M. Ishida, T. Nakajima, Y. Honda, O. Kitao, H. Nakai, T. Vreven, J.A. Montgomery Jr., J.E. Peralta, F. Ogliaro, M. Bearpark, J.J. Heyd, E. Brothers, K.N. Kudin, V.N. Staroverov, R. Kobayashi, J. Normand, K. Raghavachari, A. Rendell, J.C. Burant, S.S. Iyengar, J. Tomasi, M. Cossi, N. Rega, J.M. Millam, M. Klene, J.E. Knox, J.B. Cross, V. Bakken, C. Adamo, J. Jaramillo, R. Gomperts, R.E. Stratmann, O. Yazyev, A.J. Austin, R. Cammi, C. Pomelli, J.W. Ochterski, R.L. Martin, K. Morokuma, V.G. Zakrzewski, G.A. Voth, P. Salvador, J.J. Dannenberg, S. Dapprich, A.D. Daniels, Ö. Farkas, J.B. Foresman, J.V Ortiz, J. Cioslowski, D.J. Fox, Gaussian 09, Gaussian, Inc., Wallingford CT, 2009 (n.d.).

[44] F.O.M.J. Frisch, G.W. Trucks, H.B. Schlegel, G.E. Scuseria, M.A. Robb, J.R. Cheeseman, G. Scalmani, V. Barone, B. Mennucci, G.A. Petersson, H. Nakatsuji, M. Caricato, X. Li, H.P. Hratchian, A.F. Izmaylov, J. Bloino, G. Zheng, J.L. Sonnenberg, M. Had, Gaussian 09, 2009, Gaussian, Inc., Wallingford CT, 2016.

[45] (a) W.J. Hehre, R. Ditchfield, J.A.J. Pople, Phys. Chem. 56 (1972) 2257–2261; (b) P.C. Hariharan, J.A. Pople, Theor. Chim. Acta 28 (1973) 213–222; (c) M.M. Francl, W.J. Pietro, W.J. Hehre, J.S. Binkley, M.S. Gordon, D.J. DeFrees, J.A.J. Pople, Chem. Phys. 77 (1982) 3654–3665.